SCIENTIFIC REPORTS

OPEN

SUBJECT AREAS:
ELECTRONIC MATERIALS AND DEVICES
MATERIALS PHYSICS
IMAGING
SPECTROSCOPY

Received
8 November 2011

Accepted
23 January 2012

Published
7 February 2012

Correspondence and requests for materials should be addressed to M.H. (haruta@eels.kuicr.kyoto-u.ac.jp)

Direct observation of crystal defects in an organic molecular crystals of copper hexachlorophthalocyanine by STEM-EELS

Mitsutaka Haruta & Hiroki Kurata

Institute for Chemical Research, Kyoto University, Uji, Kyoto 611-0011, Japan.

The structural analysis of crystal defects in organic thin films provides fundamental insights into their electronic properties for applications such as field effect transistors. Observation of crystal defects in organic thin films has previously been performed at rather low resolution by conventional transmission electron microscopy based on phase-contrast imaging. Herein, we apply for the first time annular dark-field imaging to the direct observation of grain boundaries in copper hexachlorophthalocyanine thin films at the atomic resolution level by using an aberration-corrected scanning transmission electron microscope combined with electron energy-loss spectroscopy. By using a low-dose technique and an optimized detection angle, we were able to visualize the contrast of light element (C and N) together with the heavier elements (Cl and Cu) within the molecular column. We were also able to identify unexpected molecular orientations in the grain boundaries along the {110} crystallographic planes giving rise to stacking faults.

Pioneering work on the high-resolution transmission electron microscopy (HR-TEM) of organic crystals was performed by Uyeda et al. in 1978 for copper hexachlorophthalocyanine ($Cl_{16}CuPc$)[1]. By applying phase-contrast TEM imaging at 500 kV, they demonstrated that molecular imaging could resolve individual chlorine and copper atoms in a molecular column. After this work, HR-TEM methods based on phase-contrast imaging have been applied to many organic crystals[2–5], revealing epitaxial growth and structural defects. However, phase-contrast imaging is very sensitive to a range of conditions including specimen thickness and defocusing of the objective lens as well as radiation damage of the specimen, and as such the analysis of defects has been limited to a lower resolution level of 0.3 to 0.4 nm.

An alternative method to obtain high-resolution images is annular dark-field (ADF) imaging using a scanning transmission electron microscope (STEM). This method has significant advantages over phase-contrast TEM such as robustness to imaging conditions and the realization of chemical contrast according to atomic number (Z) owing to incoherent imaging[6]. We were the first to apply the low-angle (LA) ADF-STEM method to thin-film organic crystals of $Cl_{16}CuPc$[7] and related molecules[8], and successfully obtained molecular images of 0.3 nm resolution. Although the chlorine and copper atomic columns could be visualized using a quantitative image contrast with $Z^{1.7}$ dependency, the light element (C and N) columns were not observed because of the rather broad incident electron probe of about 0.2 nm, which led to unnecessary irradiation damage by the tail of the probe and limiting of the potential magnification. In order to overcome this problem, we recognized the necessity of a smaller electron probe in providing atomic resolution images suitable for defect analysis as well as for visualization of the light elements.

Over the last decade, developments in spherical aberration correctors for illuminating lens systems have significantly improved the probe size and spatial resolution of ADF-STEM images[9], enabling visualization of individual atomic columns in a crystal. For specimens consisting of only light elements like boron nitride[10] or graphene[11], atomic resolution ADF imaging has been achieved using a low accelerating voltage STEM equipped with a spherical aberration corrector for the illuminating lens system. Very recently, the direct imaging of hydrogen atomic columns in VH_2[12] and YH_2[13] was reported using a new imaging technique, called annular bright-field (ABF) STEM imaging. In the present work, we aimed to perform higher resolution molecular imaging and analyze the structural defects in an organic thin film of $Cl_{16}CuPc$ by direct observation of the molecular columns using ABF and ADF-STEM combined with electron energy-loss spectroscopy (EELS).

Results

Figure 1(b) shows a typical low-magnification image of a $Cl_{16}CuPc$ (Fig. 1(a)) crystal projected along the *c*-axis by tilting the sample about 26.5 degree around *b*-axis. The crystal habit is formed by {110} planes of the $Cl_{16}CuPc$ crystal, and some defects and holes, caused by impurities of mainly CuO and Cu_2O, are observed in the crystal as previously reported by Smith et al.[14]. Figure 1(c) shows a high-magnification LAADF-STEM image of $Cl_{16}CuPc$ obtained from a single crystal region. The brightest dots in the image correspond to the copper atomic columns for each molecular unit. Figures 1(d) and (e) show a LAADF-STEM image of one molecular column, which is translationally averaged over four molecular columns, and its noise-filtered image, respectively. It should be noted that the contrast allowed for successful observation of the benzene and porphyrin rings made up of light elements (C and N) together with the heavier elements (Cl and Cu), even in the experimental averaged image. These light elements were not observed in our previous research when LAADF-STEM was used without a spherical aberration corrector[7,8]. The improvements in resolution and signal-to-noise ratio are a result of the high current density of the fine electron probe obtained by spherical aberration correction, which had also been reported[15]. Additionally, since unnecessary irradiation was minimized by using a sub-angstrom probe as suggested in our previous research[7], high-magnification imaging could be performed, which allowed recognition of individual atoms in a molecule. Therefore, complete molecular imaging with Z-contrast was achieved at atomic resolution using LAADF-STEM combined with a spherical aberration corrector.

ABF-STEM images[12] were also taken as shown in Fig. 1(f) and (g). In the ABF images, which show the atomic columns as dark contrast, detailed molecular imaging was also achieved, and the carbon and nitrogen atomic columns of the benzene and porphyrin rings were clearly resolved, which indicates a spatial resolution better than 0.14 nm (see Supplementary Information). Since the ABF-STEM method has already provided images of hydrogen atomic columns[12,13], the prospect of complete atomic imaging of a molecular crystal, including the hydrogen atoms, appears within reach for a range of materials.

As a next step, the crystal defects as indicated by black arrows in Fig. 1(b) were investigated using LAADF-STEM combined with EELS. Figure 2(a) shows a typical stacking fault along the $(1\bar{1}0)$

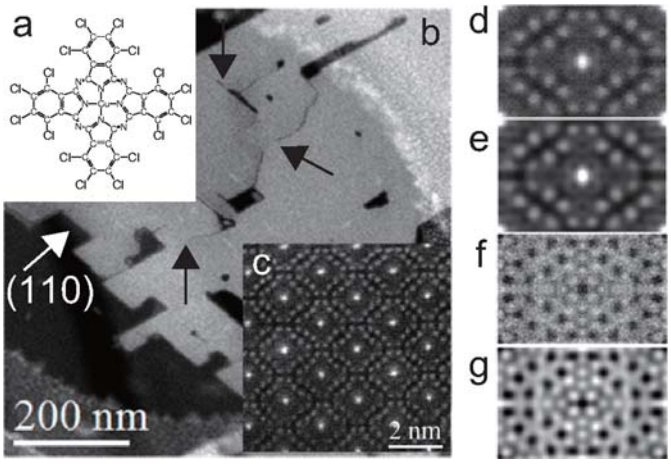

Figure 1 | (a) Molecular structure of $Cl_{16}CuPc$. (b) Low-magnification image of $Cl_{16}CuPc$ molecular crystal projected along the *c*-axis. (c) High-resolution LAADF-STEM raw image from a single crystal region. (d) Translationally averaged experimental and (e) noise-filtered LAADF-STEM images of one molecular column. (f) Translationally averaged experimental and (g) noise-filtered ABF-STEM images of one molecular column.

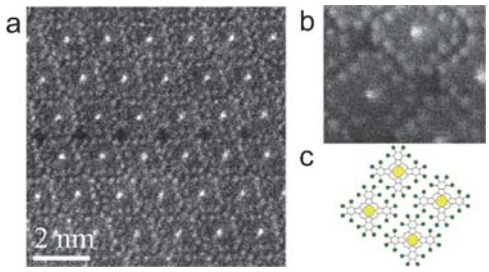

Figure 2 | (a) LAADF-STEM image showing a typical stacking fault along the $(1\bar{1}0)$ crystallographic plane. (b) High-magnification image around the stacking fault. (c) Schematic diagram of molecular packing around the stacking fault.

crystallographic plane, in which the molecular domains are shifted with respect to each other by 0.52 nm along the boundary, while the molecular orientation in each domain is maintained, as reported in previous work[14]. Periodic vacant spaces can be seen along the grain boundary. The high-magnification image (Fig. 2(b)) demonstrates that the molecular packing around the boundary can be accurately determined at the atomic level as illustrated in Fig. 2(c). The vacant spaces are surrounded by four chlorine atoms. In this location, there are no additional molecules or impurities in the grain boundary, which is the same result as that reported in previous work[14]. However, additional molecules were often observed to fill the spaces in other grain boundaries. Figures 3(a) and (b) show an LAADF-STEM image and a schematic diagram of the molecular arrangement, respectively, in which the two grain boundaries cross at point X. The crystal domains A and B contact each other along the XX' and XY boundaries, while both crystal domains are superimposed at region C, which is confirmed by the close proximity of the copper atomic columns indicated by the black arrows. The XX' grain boundary is along the (110) plane, while the XY boundary is along the $(1\bar{1}0)$ plane. At the XX' boundary, domain A shifts by 0.52 nm relative to domain B, which is similar to the structure at the boundary observed in Fig. 2(a), with the exception of the superposition of domains A and B. Additional molecules with irregular orientation can also be observed at the XY boundary as line contrasts. This line contrast is attributed to molecules oriented parallel to the *c*-axis of the crystal, which was confirmed by EELS measurements as discussed later. Since the line contrast in the grain boundary is clearly observed in the image, it is considered that the molecules may be stacking along the *c*-axis to form a column. The existence of molecules with irregular orientation in the grain boundary along the $(1\bar{1}0)$ plane might lead to a stacking fault in the (110) plane between the

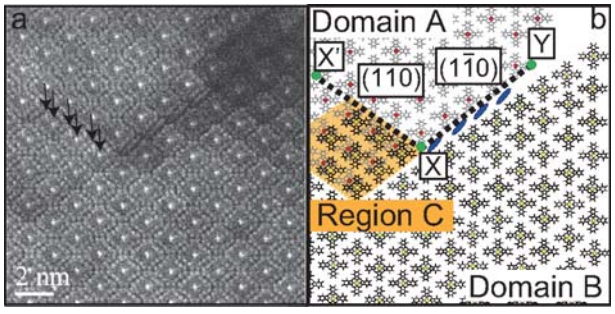

Figure 3 | (a) LAADF-STEM image of complex defect region. The stacking fault was observed along the (110) plane and $Cl_{16}CuPc$ molecules with irregular orientation were identified in the grain boundary along the $(1\bar{1}0)$ plane as a line contrast. (b) Schematic diagram of molecular columns corresponding to (a). The two domains, A and B, can be seen as gray and black molecules, and molecules along the XY grain boundary are shown as blue ellipses.

two crystal domains (shown as gray and black molecules, respectively, in Fig. 3(b)).

Molecules with irregular orientation were often observed to fill spaces along the grain boundary when the boundary width between the two domains was narrower than the planar size of a molecule as shown in Fig. 4(a) and (b). In these images two or three molecules can be observed at the boundary with an intermolecular distance of approximately 0.36 nm, which is almost the same distance as the *c*-axis spacing (0.368 nm) of the Cl_{16}CuPc molecular crystal[14]. Interestingly, each molecular plane observed as a line contrast is not parallel to the {110} crystallographic plane but deviates slightly from the plane, which suggests there are specific interactions between the molecules in the grain boundary and the peripheral chlorine atoms of the edge molecules of both grains.

Discussion

EELS measurements were conducted to confirm the orientation of the molecules observed in the grain boundaries[16]. Figure 4(c, d) shows the carbon K-edge spectra obtained from the bulk region (a) and grain boundary (b). The spectra were aligned at pre-peak position. These spectra exhibit fundamentally different shapes. In particular, the pre-peak in the spectrum of the grain boundary (Fig. 4(d)) was stronger than that of the bulk region (Fig. 4(c)).

The pre-peak of the C K-edge is attributed to the transitions of 1s electrons of carbon into the unoccupied π* states of the Cl_{16}CuPc molecules. Since the π* states consist of 2p atomic orbitals of carbon directed out-of-plane to the molecules ($2p_z$), the intensity of the pre-peak reflects the molecular orientation with respect to the direction of momentum transfer upon excitation[17]. In our STEM-EELS experiment, the momentum transfer is mostly confined to lie in the plane perpendicular to the electron beam direction[18–20]. Thus if the molecular plane is perpendicular to the electron beam, the pre-peak intensity should be weak because the direction of the $2p_z$ orbitals is perpendicular to the momentum transfer. Since the plane of molecules in the grains is tilted at an angle of 63.5 degree to the electron beam, the spectrum measured from the bulk region shows a rather weak pre-peak, as shown in Fig. 4(c). Therefore, the strong pre-peak intensity measured from molecules in the grain boundary (Fig. 4(d)) is evidence that the plane of molecules in that region is parallel to the electron beam as shown by the line contrast in the images. The reason for such irregular orientation of molecules in the grain boundaries is not clear but may relate to local interactions between the molecules and the substrate surface[21].

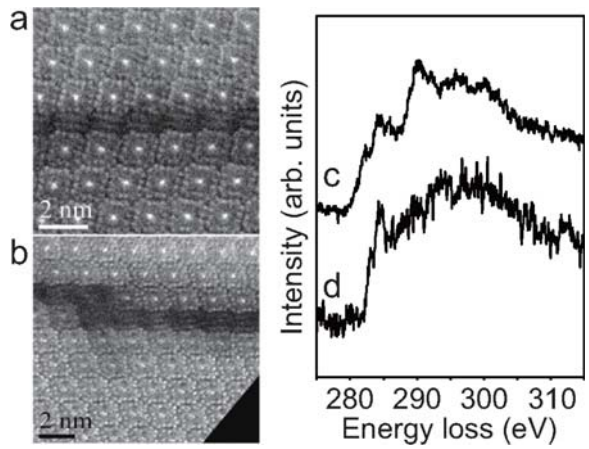

Figure 4 | LAADF-STEM image showing (a) two or (b) three Cl_{16}CuPc molecules intervening in the space between two grains having a {110} crystal habit. Carbon K-edge spectrum of Cl_{16}CuPc measured from (c) bulk region and (d) grain boundary. The spectra were aligned at pre-peak position.

In summary, by using a low-dose technique and an optimized detection angle for annular dark-field imaging, we attained a resolution better than 0.18 nm in organic molecular imaging, and were able to visualize nitrogen atomic columns within the molecular column. The results clearly show that the grain boundary parallel to the {110} plane is filled by the molecules with irregular orientation compared to the molecules in the grains. Having such a structure in the grain boundary would affect the properties of the organic thin films. Thin films of Cl_{16}CuPc molecules were reported to exhibit a field-effect transistor (FET) performance almost comparable to F_{16}CuPc with good air stability[22]. The FET performance of thin films, however, is generally low compared to that of a single crystal. This poorer performance results from grain boundaries, defects and impurities in the films, which masks the intrinsic FET properties. Thus direct observation of the grain boundary structure as shown herein can illuminate the relation between the overall properties of organic thin-film transistors and the quality of the underlying crystal.

Methods

Microscopy. The thin organic crystals were observed at room temperature by a spherical aberration corrected STEM (JEM-9980TKP1; accelerating voltage = 200 kV, $C_s = -0.025$ mm, $C_5 = 15$ mm) equipped with a nano-tip cold emission gun (FEG), consisting of a nano-protrusion on a tip apex of W<111> emitter[23], and combined with an omega-filter for EELS measurements. EEL spectra were measured with a collection semi-angle of 25 mrad. The energy resolution measured by the full width at half maximum of a zero-loss peak was about 0.5 eV. Here, the annular detection angle for ADF was set to 39–104 mrad, corresponding to low-angle annular dark-field (LAADF) imaging rather than high-angle (HA) ADF-STEM (typical detection inner angle: more than 50 mrad). In our previous research, it was reported that LAADF imaging was beneficial for improving the signal-to-noise ratio under incoherent condition for organic crystals because of the large size of the unit cell and the large Debye-Waller factor as compared with those of inorganic crystals[7,8] as discussed supplementary information. For ABF imaging the detection angle was set to 11–23 mrad because the convergent semi-angle of the incident probe was 23 mrad[12,13]. The incident electron probe was 0.1 nm or less in diameter with a probe current of less than 1 pA. The probe current fallen on the small phosphorous-viewing screen was measured using an ammeter, which was calibrated by a Faraday cup previously. Image processing was performed by Fourier filtering, where a circular mask of 16 nm^{-1} in diameter cut out high spatial frequencies from the images. And then, the filtered images were translationally averaged. Processing images are shown in Figs. 1(e) and (g). The EEL spectra were obtained by summing several spectra from equivalent region to improve the signal-to-noise ratio. In order to avoid electron damage to the specimen, each spectrum was acquired by scanning electron probe with high speed and short acquisition time. The electron dose for EELS was ca. 20 C cm^{-2}, which is less than the critical dose (ca. 35 C cm^{-2}) for the Cl_{16}-CuPc crystal[24].

Sample preparation. Thin-film specimens of Cl_{16}-CuPc were prepared on a (001)-cleaved surface of single-crystal KCl by vacuum deposition[24]. The thickness of thin film was approximately 30–40 nm measured by AFM. The temperature of the substrate was maintained at 320°C during deposition. After deposition, samples of the Cl_{16}-CuPc crystallites were covered with a very thin amorphous carbon film as a support. The KCl substrate was then removed on a surface of distilled water and the floating crystals covered with carbon film were fixed on a microgrid.

1. Uyeda, N. Kobayashi, T. Ishizuka, K. & Fujiyoshi, Y. High voltage electron microscopy for image discrimination of constituent atoms in crystals and molecules. *Chem. Scripta.* **14**, 47–61 (1978–1979).
2. Kobayashi, T. in: N. Karl (Ed.), Epitaxial growth of organic thin films and characterization of their defect structures by high-resolution electron microscopy. *Crystal, Growth, Properties and Application*, vol. 13, Springer, Berlin, Heidelberg, 1991, p. 2.
3. Uyeda, N. Kobayashi, T. Ishizuka, K. & Fujiyoshi, Y. Crystal structure of Ag TCNQ. *Nature.* **285**, 95–97 (1980).
4. Maeda, T. Isoda, S. & Kobayashi, T. Epitaxial growth and defect Structure of quaterrylene studied using high resolution electron microscopy. *Phys. Status Solidi* (a) **191**, 489–498 (2002).
5. Koshino, M. Kurata, H. & Isoda, S. Study of structures at the boundary and defects in organic thin films of perchlorocoronene by high-resolution and analytical transmission electron microscopy. *Ultramicroscopy.* **110**, 1465–1474 (2010).
6. Pennycook, S. J. & Jesson, D. E. High-resolution incoherent imaging of crystals. *Phys. Rev. Lett.* **64**, 938–941 (1990).
7. Haruta, M. Yoshida, K. Kurata, H. & Isoda, S. Atomic resolution ADF-STEM imaging of organic molecular crystal of halogenated copper phthalocyanine. *Ultramicroscopy.* **108**, 545–551 (2008).

8. Haruta, M. Yoshida, K. Kurata, H. & Isoda, S. High resolution ADF-STEM imaging application for organic crystals. *Mol. Cryst. Liq. Cryst.* **492**, 200–209 (2008).
9. Batson, P. E. Delby, N. & Krivanek, O. L. Sub-ångstrom resolution using aberration corrected electron optics. *Nature.* **418**, 617–620 (2002).
10. Krivanek, O. L. *et al*. Atom-by-atom structural and chemical analysis by annular dark-field electron microscopy. *Nature.* **464**, 571–574 (2010).
11. Suenaga, K. & Koshino, M. Atom-by-atom spectroscopy at graphene edge. *Nature.* **468**, 1088–1090 (2010).
12. Findlay, S. D. *et al*. Direct imaging of hydrogen within a crystalline environment. *Appl. Phys. Express.* **3**, 116603 (2010).
13. Ishikawa, R. *et al*. Direct imaging of hydrogen-atom columns in a crystal by annular bright-field electron microscopy. *Nature mater*. **10**, 278–281 (2011).
14. Smith, D. J. Fryer, J. R. & Camps, R. A. Radiation damage and structural studies: halogenated phthalocyanines. *Ultramicroscopy.* **19**, 279–297 (1986).
15. Pennycook, S. J. & Nellist, P. D. *Scanning transmission electron microscopy : imaging and analysis* (Springer, New York, 2011).
16. Hashimoto, S. Isoda, S. Kurata, H. Lieser, G. & Kobayashi, T. Molecular orientation of perfluoro-vanadyl-phthalocyanine examined by electron energy loss spectroscopy. *J. Porphyrins and Phthalocyanines*, **3**, 585–591 (1999).
17. Kurata, H. Ishizuka, K. Kobayashi, T. & Uyeda, N. Orientation dependence of the carbon K-edge in the electron energy loss spectra of a potassium-benzene-graphite intercalation compound. *Synthetic Metals.* **22**, 337–348 (1988).
18. Browning, N. D. Yuan, J. & Brown, L. M. Real-space determination of anisotropic electronic structure by electron energy loss spectroscopy. *Ultramicroscopy.* **38**, 291–298 (1991).
19. Batson, P. E. & Chisholm, M. F. Anisotropy in the near-edge absorption fine structure of $YBa_2Cu_3O_{7-\sigma}$. *Phys. Rev. B* **37**, 635–637 (1988).
20. Batson, P. E. Carbon 1s near-edge-absorption fine structure in Graphite. *Phys. Rev. B* **48**, 2608–2610 (1993).
21. Tokito, S. Sakata, J. & Taga, Y. The molecular orientation in copper phthalocyanine thin films deposited on metal film surfaces. *Thin Solid Films.* **256**, 182–185 (1995).
22. Ling, M. M. Bao, Z. & Erk, P. Air-stable n-channel copper hexachlorophthalocyanine for field-effect transistors. *Appl. Phys. Lett.* **89**, 163516 (2006).
23. Kurata, H. Isoda S. & Tomita, T. *Proc. of the 16th International Microscopy Congress (IMC16)*, Sapporo, Japan, p. 583. (2006).
24. Kurata, H. Isoda S. & Kobayashi, T. EELS study of radiation damage in chlorinated Cu-phthalocyanine and poly GeO-phthalocyanine. *Ultramicroscopy*, **41**, 33–40 (1992).

Author contributions

M. H. and H. K initiated and designed the research and, interpreted the date and wrote the paper. M. H designed the experiments.

Additional information

Supplementary information accompanies this paper at http://www.nature.com/scientificreports

Competing financial interests: The authors declare no competing financial interests.

How to cite this article: Haruta, M. & Kurata, H. Direct observation of crystal defects in an organic molecular crystals of copper hexachlorophthalocyanine by STEM-EELS. *Sci. Rep.* **2**, 252; DOI:10.1038/srep00252 (2012).